Channel switching in above-threshold ionization of xenon

V. Schyja, T. Lang, and H. Helm
Department of Molecular and Optical Physics, Albert-Ludwigs-Universität, 79104 Freiburg, Germany
(Received 18 August 1997)

The intensity dependence of the angular and energy distributions of photoelectrons is used to map the effect of channel closing in short-pulse, multiphoton ionization of xenon. At 800 nm, we observe the nine-photon channel to close at $\approx 3\times 10^{13}$ W/cm^2 and the dominant ionization path to switch from $(8+1)$-photon resonant ionization via f-type Rydberg states to $(9+1)$-photon resonant ionization via g-type Rydberg states. Very low-energy electrons are observed prior to reaching the channel closing intensity, indicative of a contribution of nonresonant ionization. [S1050-2947(98)02201-X]

PACS number(s): 32.80.Rm, 33.80.Rv, 42.50.Hz

I. INTRODUCTION

The study of photoionization at laser intensities above 1 TW/cm^2 has been an active topic of research over the past 20 years. After the discovery [1] of above-threshold-ionization (ATI) fine structure within each ATI order was discovered and attributed to transient resonance of ac Stark shifted Rydberg states at specific intensities within the laser pulse [2,3]. Recent work has concentrated on the high-energy portion of the photoelectron spectrum, which displays plateau and jet-features [4–7]. These features are in part attributed to elastic backscattering of a revisiting photoelectron from its parent ion.

Little work has been reported on the intensity dependence of the photoelectron energy spectrum at the lowest intensities, where backscattering is considered insignificant (in xenon below $\approx 5\times 10^{13}$ W/cm^2). Here we present data on the resonant behavior of ATI that shows that channel closing due to ponderomotive shifting leads to switching between intermediate resonances of even and odd parity. This switching is indicated schematically in the energy diagram in Fig. 1. At 800 nm eight photons are required to reach the continuum at zero intensity. However, the Stark shift increases the ionization potential with intensity such than nine photons are required at $\approx 4\times 10^{12}$ W/cm^2. At this low intensity ionization is still highly improbable and only near $\approx 1\times 10^{13}$ W/cm^2 is ionization efficient enough to accumulate spectra within a reasonable time period. In this low-intensity regime excited states are tuned into resonance with the eight-photon dressed ground state and excitation occurs to Xe* states from which the continuum can be reached with one photon. In the short pulse case the energy signature of these photoelectrons is closely approximated by a picture that assumes ponderomotive shifting of the excited state as well as the ionization threshold, hence the electron energy is $E_e \approx h\nu - V_{\mathrm{ion}}(\mathrm{Xe}^*)$. In Fig. 1 such a transition is shown for eight-photon resonance. This $(8+1)$-photon channel closes eventually as the intensity is increased further. Channel switching to $(9+1)$-photon ionization occurs at higher intensity as shown in Fig. 1 at the example of the Xe($5g$) state. This switching is analogous to findings in helium and neon reported in our earlier work [8,9]. This switching has been predicted in theoretical work on MPI of atomic hydrogen [10] and has been observed to occur in xenon [11] when changing wavelength to select even and odd parity resonances.

II. EXPERIMENTAL AND RESULTS

A photoelectron imaging spectrometer [12] is used to monitor the angular and energy distribution of photoelectrons formed in the focus of a laser beam. The focal region represents a point source of photoelectrons. While expanding from this origin, a dc electric field (ranging from 10 to 400 V/cm) projects the electrons onto a 50-mm diameter multi-

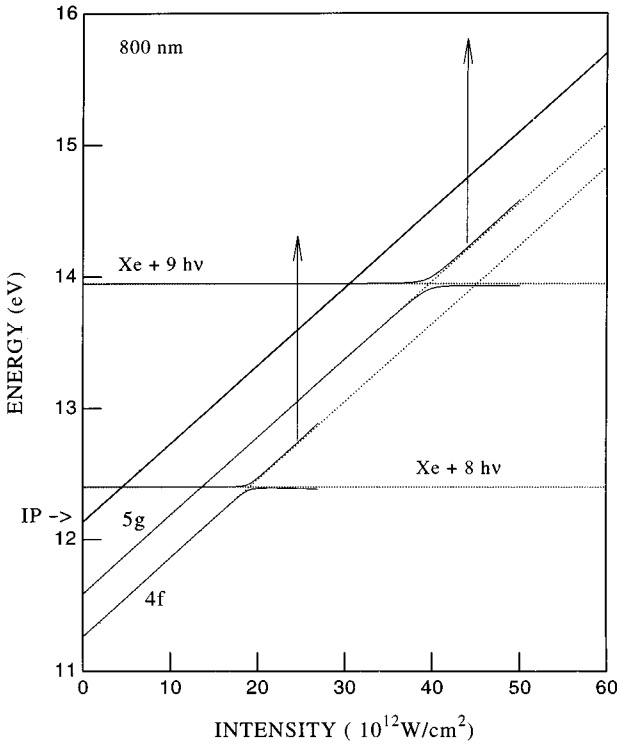

FIG. 1. Schematic diagram of resonance shifting and channel switching in xenon at 800 nm. For reasons of clarity only the $4f$ and $5g$ states are indicated. A large, arbitrary N-photon matrix element was chosen to accentuate the avoided crossing of the $(N=8)$-photon dressed ground state and the ponderomotively shifted $4f$ state as well as the $(N=9)$-photon dressed ground state and the equally shifted $5g$ state.

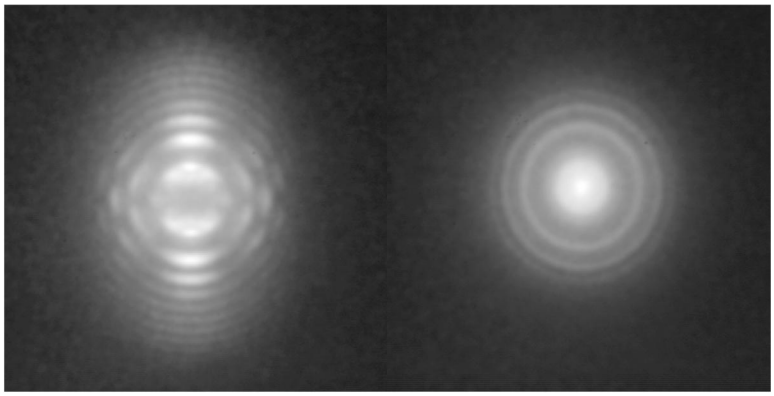

FIG. 2. Raw photoelectron image recorded with vertical laser polarization, oriented parallel to the page is shown on the left. An image recorded under otherwise identical conditions, but with the laser polarization oriented perpendicular to the page is shown on the right.

channel plate with phosphor screen attached. A video camera records impact positions of the photoelectrons. In a single shot typically 10–100 electron positions are recorded. To achieve this the xenon pressure is adjusted between 5×10^{-7} to 1×10^{-5} Torr when the laser energy is varied from 4 to 40 μJ. Pending on the complexity of the image the impacts of 10^4-10^5 electrons are accumulated in a PC-stored image.

A Ti-sapphire laser with chirped-pulse amplifier at a 1-kHz repetition rate is used in this study. The duration of the amplified pulse is monitored by an interferometric autocorrelator as well as a FROG and lies typically at 100 fs. The pulse energy is varied using a half-wave plate and polarizing beam splitter. The laser wavelength is centered around 800 nm with a full width at half maximum (FWHM) of 9 nm. An $F4$ lens of 150-mm focal length is used to focus the laser beam. The peak laser intensity is calibrated relative to the intensity where the Xe($4f$) state shifts into eight-photon resonance. In this calibration we assume that the $4f$ state shifts ponderomotively [3,13]. With this assumption the $4f$ state is tuned into resonance at 1.8×10^{13} W/cm^2 at 800 nm.

Figure 2 shows raw photoelectron images representative for ionization of xenon at 2.2×10^{13} W/cm^2. To record the image on the left, the laser polarization was oriented vertical and parallel to the screen. The image is formed from the projection of concentric shells of ATI electrons with discrete energy, the groups being separated by the one-photon energy. Since the spatial expansion of a sphere of monoenergetic electrons on the way to the screen proceeds in proportion to the initial velocity of the electron, the spacing between ATI shells progressively decreases as the ATI number increases. Viewing these electron spheres with the laser polarization oriented perpendicular to the screen reveals rotational symmetry of the emitted electrons around the direction of linear laser polarization. The image on the right in Fig. 2 was recorded with the laser polarization perpendicular to the screen under otherwise identical conditions. The symmetry of electron ejection around the polarization axis is evident.

Images such as shown in Fig. 2 can be deconvoluted in an Abelian transformation [12,14] to yield angle-resolved velocity distributions of the photoelectrons. Typical samples showing the intensity dependence of these distributions are shown in Fig. 3. The intensity increases from 1.2×10^{13} to 4×10^{13} W/cm^2 when going from Fig. 3(a) to 3(f). In these deconvoluted images the distance from the center of the image is proportional to the electron velocity while the brightness along a circular portion depicts the electron angular distribution.

III. DISCUSSION

A. (8+1)-photon ionization

We begin with a discussion of the deconvoluted images given in Fig. 3. The experimental conditions for projecting the electrons are identical in all images shown; merely laser intensity and xenon pressure are varied. In Fig. 3(a), at 1.2×10^{13} W/cm^2, a sequence of discrete peaks at energies corresponding to one-, two-, three-, etc. photon ionization of excited xenon atoms dominates the image. The concentric rings are spaced by the photon energy (1.55 eV), the lowest ring peaking at $\approx$1.20 eV, corresponding to the energy that is expected for one-photon ionization of ponderomotively shifted Xe($10p$) and/or Xe($6f$) states (1.22 and 1.16 eV, respectively). The angular distribution of the innermost ring (corresponding to the lowest-order peak) shows profound intensity near 90° relative to the laser polarization. This is a unique identification that even-l partial waves contribute to outgoing photoelectron, as expected for ionization from an odd-l resonant intermediate state. The next larger ring feature corresponds to the first ATI peak, i.e., $(8+2)$-photon ionization. Here a clear minimum in electron intensity is observed at 90°. This is also consistent with an odd-l resonant intermediate since the additional absorption of one photon requires the l value of partial waves that contribute to the photoelectron signal to change by ±1. This change in l character appears throughout all ATI series.

In Fig. 3(b) the intensity is increased to 1.9×10^{13} W/cm^2. We recognize that the lowest-energy contribution now forms a ring of smaller diameter, indicative of lower electron energy. This distribution peaks at an energy of 0.68 eV, as expected for ionization via the Xe($4f$) state. A fainter contribution at larger radius (higher energy) is also visible. It is associated with the energetically higher-lying states ($5f$). Angle-integrated velocity distributions from the images shown in Fig. 3 were converted into energy distributions and are shown in Fig. 4. The reduction in the location of the dominant photoelectron peak when going from 1.2×10^{13} to 1.9×10^{13} W/cm^2 is evident. Upon raising the in-

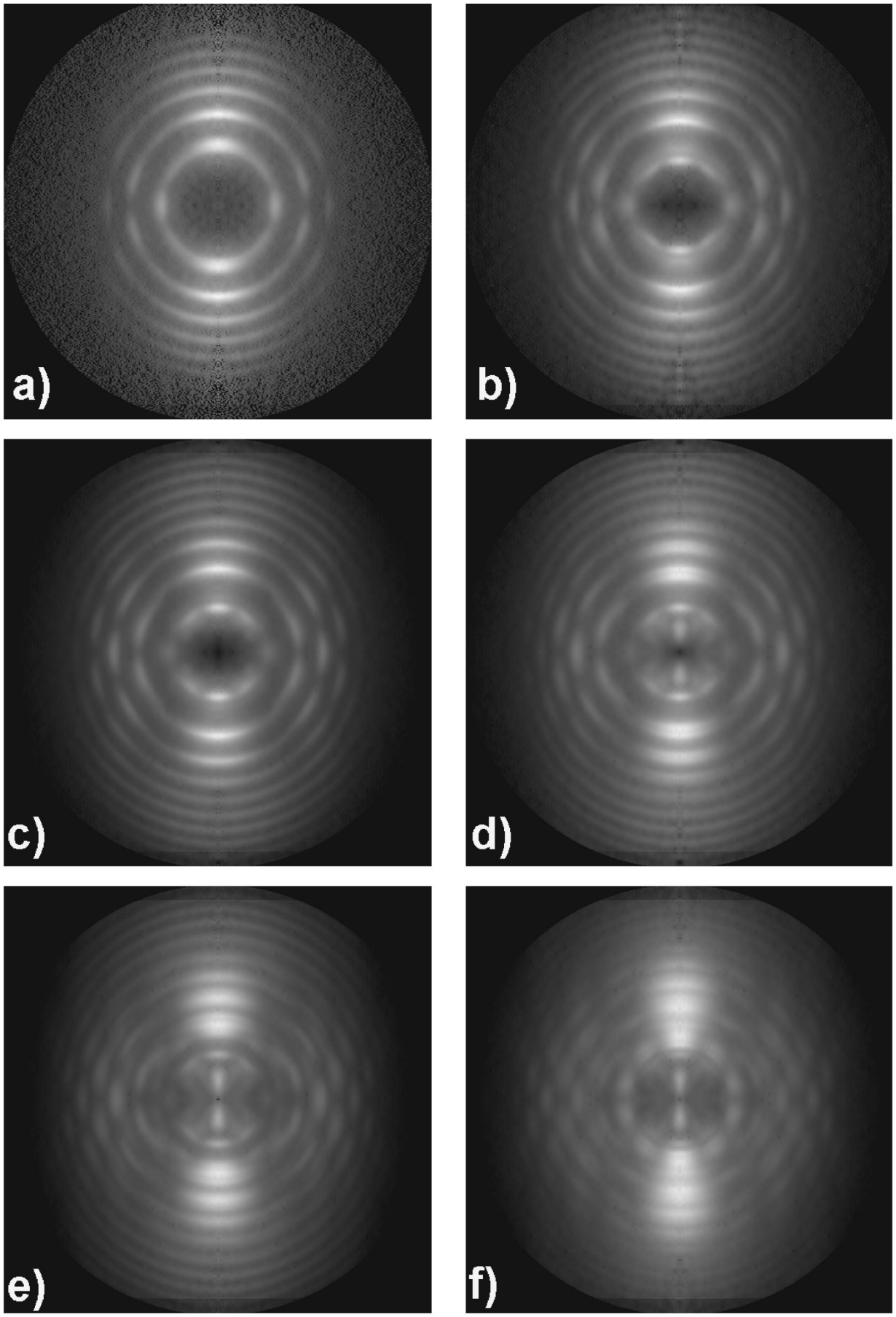

FIG. 3. Deconvoluted photoelectron images recorded at various intensities (W/cm^2). (a) 1.2×10^{13}, (b) 1.9×10^{13}, (c) 2.0×10^{13}, (d) 2.5×10^{13}, (e) 3.5×10^{13}, (f) 4.0×10^{13}.

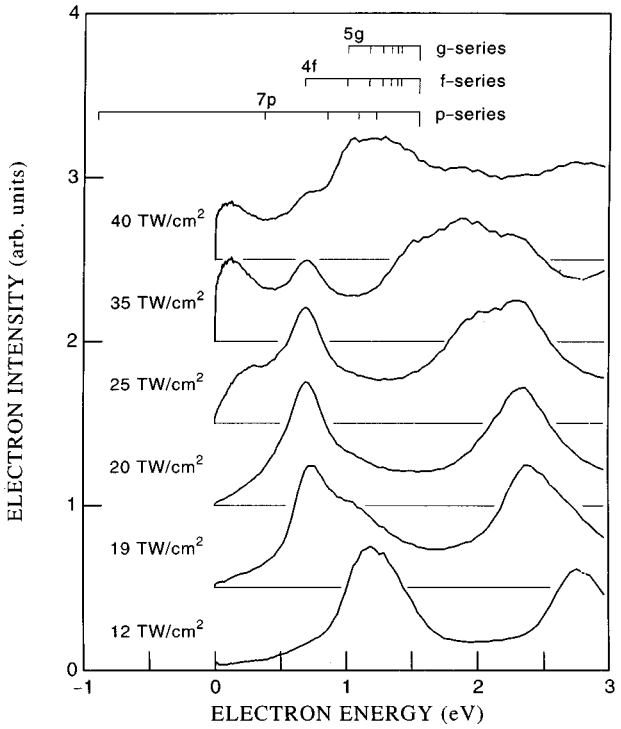

FIG. 4. Angle-integrated and normalized photoelectron energy distributions at the intensities given in Figs. 3(a) to 3(f). In order to obtain relative electron intensities, the scales have to be multiplied by 1, 7, 8, 9, 50, and 250 for 12, 19, 20, 25, 35, and 45 TW/cm^2, respectively.

tensity to 2.0×10^{13} W/cm^2 the $4f$-state contribution dominates in the lowest ionization channel as well as the respective ATI peaks [Fig. 3(c)]. The angular distribution corresponding to the $4f$ state in Fig. 3(b) and 3(c) displays four pronounced nodal planes in the angular distribution. This is a clear sign that partial waves at least up to $l=4$ (g waves) contribute to this photoelectron channel.

The $4f$ states are the lowest-lying, high-l levels that can be shifted into eight-photon resonance at 800 nm. In principle, the $7p$ state of xenon is available on grounds of parity and energy, however, an increase in intensity does not result in a corresponding appearance of an energy and angular distribution that is commensurate with resonant ionization via a ponderomotively shifted $7p$ state. Rather, a continuous distribution of electron energies lying lower than the $4f$ peak is observed to add to the photoelectron image as the intensity is increased. This effect is apparent from Fig. 3(d), which was recorded at an intensity of 2.5×10^{13} W/cm^2. Most importantly, the angular distribution associated with this feature reveals at least six nodal planes, a feature that is not commensurate with one-photon ionization from an intermediate with p character. A possible origin of this ionization channel is nonresonant ionization, the decreasing electron energy resulting from the increased spacing between ground state and the ionization threshold $Xe^+(^2P_{3/2})$ as the intensity increases. We note that this group of low-energy electrons appears in previous calculations on atomic hydrogen [10] and xenon [18], and has been shown to occur in the respective experimental distributions [15,11].

As the intensity is further increased [Figs. 3(e) and 3(f)] the lowest-energy contribution shifts progressively to lower electron energies. Below 300 meV a yet different angular distribution pattern occurs, a pronounced lobe pointing along the laser polarization. We attribute this group of electrons to above-barrier ionization of resonant excited states. To justify this origin we note that xenon excited to the $4f$ state has an ionization potential, $V_{\rm ion}(4f)=0.87$ eV. Hence the Keldysch parameter [5] for excited xenon is as low as $\gamma=[V_{\rm ion}(4f)/2U_p]^{0.5}=0.5$ at 2.5×10^{13} W/cm^2. The highest probability for escape by above-barrier ionization occurs near the crest of the electric field of the laser field. When emitted near the maximum of the E field an electron with zero kinetic energy is expected under short pulse conditions [5]. We also note that this electron group lacks an obvious feature corresponding to above-threshold ionization.

B. (9+1)-photon ionization

A dramatic modification of the electron image occurs when changing from 3.5×10^{13} to 4.0×10^{13} W/cm^2 [going from Fig. 3(e) to Fig. 3(f)]. It is the appearance of a discrete series of closely spaced peaks with an angular distribution of 5 nodal planes. Their energy lies in the range from just below the one-photon energy down to an energy of 1.0 eV. This energy location and the angular distribution uniquely identify this group of photoelectrons to resonant ionization via states with $l=4$ character. The intensity at which this feature appears shows that this ionization channel opens when the nine-photon energy falls below the ionization threshold (closing of the nine-photon channel is expected at 3.0×10^{13} W/cm^2 at 800 nm). We attribute these new features to resonant ionization via ng states. The lowest of these, Xe($5g$), lies at 11.59 eV above the ground state [16] and this state will give rise to photoelectrons with 1-eV electron energy when ionized with 800-nm light. In our previous studies of neon and helium shorter wavelengths were employed (308–335 nm) and six- and seven-photon ionization was required to reach just above the respective ionization thresholds. An analogous switching from even-l resonances to nonresonant ionization to odd-l resonances was observed in helium, neon, and argon [8,9,17].

This sequence of ionization features indicates that at the pulse lengths used here ionization is not saturated in xenon at intensities as high as 4.0×10^{13} W/cm^2 at 800 nm. Rather, a substantial portion of xenon atoms must survive to experience this intensity in order to participate in the resonant ionization via levels that are shifted by much more than the one-photon energy from their zero-intensity position. In order to resonantly reach the $5g$ state at 800 nm an ac Stark shift of over 2.3 eV is required.

C. Angular distribution of ATI electrons

The angular distributions of photoelectrons are summarized in Fig. 5. Here we have collected electrons with an energy falling into intervals of 200-meV width into single angular distributions. The size of each polar plot is taken proportional to the square root of the number of photoelectrons that appear in the respective energy range. This allows us to show the often peculiar angular distributions that appear for weak-ionization features. Figure 5 only shows the contribution of photoelectrons in the energy range below the first ATI peak.

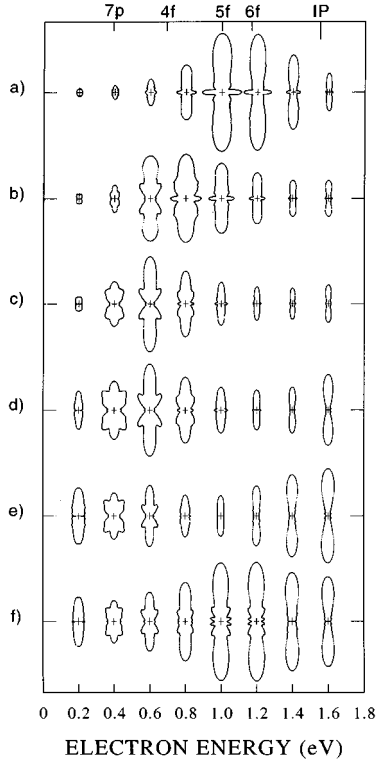

FIG. 5. Photoelectron angular distributions binned into 200-meV intervals recorded at the intensities given in Figs. 3(a) to 3(f).

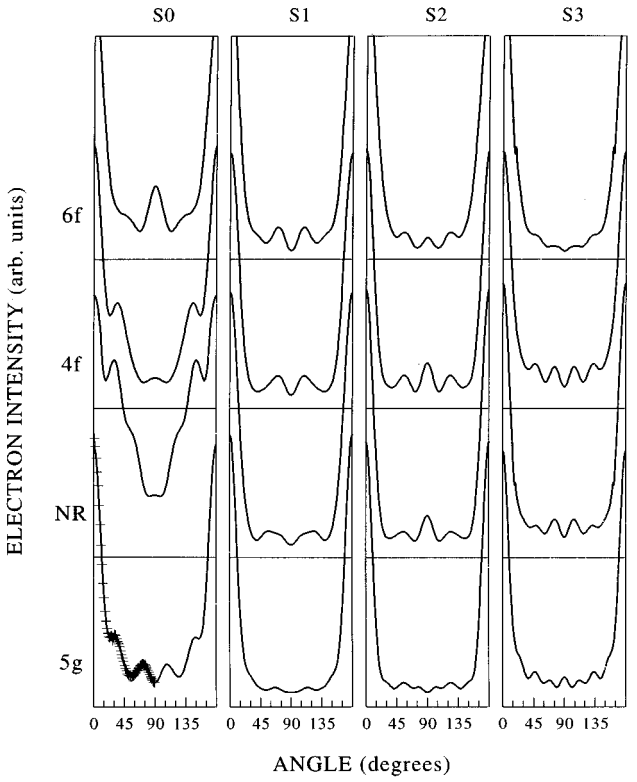

FIG. 6. Development of angular distribution within a given ATI series. (a) $4f$ at 2.0×10^{13}, (b) $6f$ at 1.2×10^{13}, (c) *nonresonant* at 2.5×10^{13} (d) $5g$ at 4.0×10^{13} W/cm^2.

Figure 6 shows individual angular distributions within the ATI series attributed to ionization via the $6f$, $4f$, and $5g$ states as well as the portion of the spectrum attributed to nonresonant ionization. The angular distributions are obtained by sampling the image intensity in an annular ring corresponding to the specified range of electron velocity over an arc segment of 1.5 to 3.0 degrees. Actual data points are given for the bottom left distribution in Fig. 6, but are left out for clarity in the remaining distributions. The general feature of an increase in the highest partial wave that contributes to the photoelectron spectrum, when proceeding within each ATI series, is apparent from these angular distributions.

Finally we note that distinct differences appear in the angular pattern of $(8+2)$-photon ionization via the Xe$(4f)$-state and $(9+1)$-photon ionization via the Xe$(5g)$ state (see Fig. 6, column $S1$,$4f$ and column $S0$,$5g$, respectively). This is further confirmation that these two 10-photon processes involve fundamentally different ionization dynamics since they occur at greatly different peak intensity.

IV. CONCLUSIONS

The observed pattern of resonance switching is consistent with all previous work in this intensity range. Moreover, the detailed development of the angular and energy distributions, including those at very low energy (<500 meV) very precisely matches the theoretical predictions of Schafer on xenon [18,19]. The interpretation and discussion of photoionization in strong laser fields involving many photons has been greatly aided by the intuitive pictures of ac Stark shifted resonances (at low intensity) and of tunnel- and above-barrier ionization (at high intensity). The observation here, that the model of ac Stark shifted resonances pertains to situations well above the channel closing intensity is a further manifestation of the validity of this picture.

Nevertheless one needs to recognize that these intuitive models are approximations and that the intensity dependence of the dynamic response of an atom to an electromagnetic wave evolves smoothly between these two extreme cases. From the point of theory the numerical solution of the time-dependent Schrödinger equation [18] is currently the most direct tool to describe this transition.

Experimentally, our imaging approach affords direct insight into the subtle details of the evolution of different ionization path an atom chooses when subjected to an intense field. A video showing the continuous development of energy and angular distribution of photoelectrons in xenon as a function of intensity is available on our web site [20].

ACKNOWLEDGMENT

This research was supported by the Deutsche Forschungsgemeinschaft under Project C14 of the SFB 276.

[1] P. Agostini, F. Fabre, G. Mainfray, and G. Petite, Phys. Rev. Lett. **42**, 1127 (1979).
[2] R. R. Freeman, P. H. Bucksbaum, H. Milchberg, S. Darack, D. Schumacher, and M. E. Geusic, Phys. Rev. Lett. **59**, 1092 (1987).
[3] P. Agostini, P. Breger, A. LHuillier, H. G. Mueller, and G. Petite, Phys. Rev. Lett. **63**, 2208 (1989).
[4] G. G. Paulus, W. Nicklich, H. Xu, P. Lambropoulos, and H. Walther, Phys. Rev. Lett. **72**, 2851 (1994).
[5] L. F. DiMauro and P. Agostini, Adv. At., Mol., Opt. Phys. **35**, 79 (1995).
[6] P. Hansch, M. A. Walker, and L. D. VanWoerkum, Phys. Rev. A **55**, R2535 (1997).
[7] M. P. Hertlein, P. H. Bucksbaum, and H. G. Muller, J. Phys. B **30**, L197 (1997).
[8] H. Helm and M. J. Dyer, Phys. Rev. A **49**, 2726 (1994).
[9] H. Helm and M. J. Dyer, in *Proceedings of the Symposium on Atomic and Molecular Physics*, edited by I. Alvarez, C. Cisneros, and T. J. Morgan (World Scientific Singapore, 1995), p. 468.
[10] M. Dörr, R. M. Potvliedge, and R. Shakeshaft, Phys. Rev. A **41**, 558 (1990).
[11] H. Rottke, B. Wolff, M. Tapernon, D. Feldmann, and K. H. Welge, Z. Phys. D **15**, 133 (1990).
[12] H. Helm, N. Bjerre, M. J. Dyer, D. L. Huestis, and M. Saeed, Phys. Rev. Lett. **70**, 3221 (1993).
[13] M. P. deBoer and H. G. Müller, J. Phys. B **27**, 721 (1994).
[14] C. Bordas, F. Pauling, H. Helm, and D. L. Huestis, Rev. Sci. Instrum. **67**, 2257 (1996).
[15] H. Rottke, B. Wolff, M. Brickwedde, D. Feldmann, and K. H. Welge, Phys. Rev. Lett. **64**, 404 (1989).
[16] S. T. Pratt, P. M. Dehmer, and J. L. Dehmer, Phys. Rev. A **35**, 3793 (1987).
[17] V. Schyja, T. Lang, and H. Helm, in *Ultrafast Processes in Spectroscopy*, edited by Swelto *et al.* (Plenum Press, New York, 1996), p. 311.
[18] K. Schafer and K. C. Kulander, Phys. Rev. A (to be published).
[19] The calculations in Ref. [18] were performed at 600 nm. However, since 8 photons of 800 nm reach the same energy range as 6 photons of 600 nm, identical resonances are involved.
[20] frhewww.physik.uni-freiburg.de (under recent highlights).